

Relations of rotation and chromospheric activity to stellar age for FGK dwarfs from Kepler and LAMOST

LIFEI YE,^{1,2} SHAOLAN BI,^{1,2} JINGHUA ZHANG,³ TIANCHENG SUN,^{1,2} LIU LONG,^{1,2} ZHISHUAI GE,⁴ TANDA LI,¹
XIANFEI ZHANG,^{1,2} XUNZHOU CHEN,⁵ YAGUANG LI,⁶ JIANZHAO ZHOU,^{1,2} AND MAOSHENG XIANG^{7,1}

¹*Institute for Frontiers in Astronomy and Astrophysics, Beijing Normal University, Beijing 102206, China*

²*Department of Astronomy, Beijing Normal University, Beijing 100875, People's Republic of China*

³*South-Western Institute for Astronomy Research, Yunnan University, Chenggong District, Kunming 650500, China*

⁴*Beijing Planetarium, Beijing Academy of Science and Technology, Beijing, 100044, China*

⁵*Research Center for Intelligent Computing Platforms, Zhejiang Laboratory, Hangzhou 311100, China*

⁶*Institute for Astronomy, University of Hawai'i, 2680 Woodlawn Drive, Honolulu, HI 96822, USA*

⁷*CAS Key Laboratory of Optical Astronomy, National Astronomical Observatories, Chinese Academy of Sciences, Beijing 100101, China*

ABSTRACT

The empirical relations between rotation period, chromospheric activity, and age can be used to estimate stellar age. To calibrate these relations, we present a catalog, including the masses and ages of 52,321 FGK dwarfs, 47,489 chromospheric activity index $\log R_{HK}^+$, 6,077 rotation period P_{rot} and variability amplitude S_{ph} , based on data from LAMOST DR7, Kepler and Gaia DR3. We find a pronounced correlation among P_{rot} , age, and [Fe/H] throughout the main-sequence phase for F dwarfs. However, the decrease of $\log R_{HK}^+$ over time is not significant except for those with [Fe/H] < -0.1. For G dwarfs, both P_{rot} and $\log R_{HK}^+$ are reliable age probes in the ranges ~ 2 -11 Gyr and ~ 2 -13 Gyr, respectively. K dwarfs exhibit a prominent decrease in $\log R_{HK}^+$ within the age range of ~ 3 -13 Gyr when the relation of $P_{rot} - \tau$ is invalid. These relations are very important for promptly estimating the age of a vast number of stars, thus serving as a powerful tool in advancing the fields of exoplanet properties, stellar evolution, and Galactic-archaeology.

Keywords: Stellar rotation (1629); Stellar activity (1580); Stellar chromospheres (230); Stellar ages (1581)

1. INTRODUCTION

Stellar age plays a crucial role in the field of planetary systems, stellar physics, Galaxy formation and evolution. The age determinations of most dwarfs are difficult because traditional model-dependent methods use stellar properties, which either change little as the star evolves or are hard to observe (Soderblom 2010). The rotation rates and activity levels of all dwarfs significantly decrease over time as these stars gradually lose their angular momentum driven by magneto stellar winds (e.g., Skumanich 1972; Noyes et al. 1984; Kawaler 1988; Matt & Pudritz 2005; Meibom et al. 2011; Metcalfe et al. 2023). When appropriately calibrated, rota-

tion period and activity proxy serve as reliable indicators of stellar ages, utilizing the methods of gyrochronology and magnetochronology. Gyrochronology and Magnetochronology are defined as relations among rotation period, activity level, mass, and age (e.g., Barnes 2003, 2007; Mamajek & Hillenbrand 2008; Vidotto et al. 2014).

Recently, the gyrochronology and magnetochronology using open clusters have been finely calibrated within 4 Gyr (e.g., Barnes 2010; García et al. 2014; Matt et al. 2015; Réville et al. 2016; Zhang et al. 2019; Angus et al. 2019; Curtis et al. 2019, 2020; Perini et al. 2021; Dungee et al. 2022; Long et al. 2023). Although the age range of near-solar metallicity dwarfs with asteroseismic parameters is expanded to ~ 10 Gyr (Angus et al. 2015; van Saders et al. 2016; Booth et al. 2020), the small sample size of data leads to oversimplified formulas that fail to account for the impact of mass and metallicity. In order to calibrate gyrochronology and magnetochronology

effectively, it is important to establish the intricate relations among rotation period, magnetic activity, mass, and age for different spectral types. This is necessary that a large sample of accurate measurements of the rotation period and magnetic activity proxies, accomplishing with reliable ages.

With the dramatically improved astrometric data from Gaia DR3 (Gaia Collaboration et al. 2022), we can now achieve high-precision luminosity. Millions of the spectra from LAMOST (Zhao et al. 2012) not only provide us with homogenous atmospheric parameters (T_{eff} , $[\text{Fe}/\text{H}]$), but also are used to measure chromospheric activity levels. Combining these observations we can obtain precise mass and age through grid-based modeling (Schaerer et al. 1993; Yi et al. 2001; Gustafsson et al. 2008; Dotter et al. 2008; Bressan et al. 2012; Choi et al. 2016; Moser et al. 2023). In addition, Kepler space mission provides the rotation period (P_{rot}) and photometric variability amplitudes (S_{ph}) for tens of thousands of stars (Basri et al. 2011; McQuillan et al. 2013, 2014; Mathur et al. 2014; Reinhold & Gizon 2015; Santos et al. 2019, 2021). Thanks to these improvements, it will provide a chance to construct a large, homogeneous, and comprehensive sample, which opens a new insight into gyrochronology and magnetochronology.

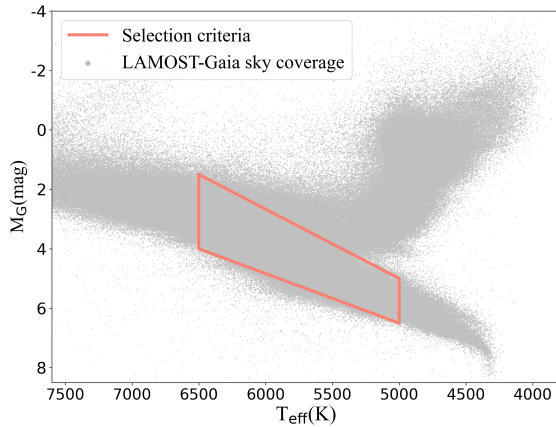


Figure 1. $T_{\text{eff}} - M_G$ diagram of the stars in the field of LAMOST and Gaia (grey dots); the orange boundary is our selection criteria according to Section.2.

This work aims to provide a catalog and explore the relations among stellar rotation, magnetic activity, mass and age. The sample selection details are in Section 2. The stellar mass and age are estimated in section 3. In Section 4, we calibrate the relations among the above parameters. Our conclusions are summarized in Section.5.

2. SAMPLE SELECTION

We use atmospheric parameters of LAMOST DR7 derived by Data-Driven Paynes (DD-Payne) approach (Xiang et al. 2019). The absolute magnitude(M_G) and luminosity are from Gaia DR3¹. The sample are selected as the following steps:

1. We set $S/N \geq 50$, $flag_{chi2}$ ² = 1, and $flag_{unique}$ ³ = 1 to obtain reliable atmospheric parameters from LAMOST DR7 data.
2. Cross-matching stars between Gaia DR3 and LAMOST DR7. Based on the crossover radius of 2 arcsecs, we obtain 1,274,433 common stars with luminosity uncertainty less than 10%, as shown as gray dots in Fig.1.
3. We adopt the following empirical formula to select the main-sequence stars in the T_{eff} range of 5000–6500 K by referring to Petigura et al. (2022):

$$M_G = -0.00233T_{\text{eff}} + 16.66667, \quad (1)$$

$$M_G = -0.00167T_{\text{eff}} + 14.83333. \quad (2)$$

the Eq.1 and Eq.2 correspond to the upper and lower boundaries, respectively. A total of 849,163 main-sequence stars are selected as shown in Fig.1;

4. We use Gaia renormalized unit weight error (RUWE) ≥ 1.2 as the criterion to remove non-single stars or astrometric noise (Rybizki et al. 2022). We also remove the non-rotation type of the International Variable Star Index⁴ (VSX) to reduce binaries or multiple systems.

Based on the above steps, we obtain 698,885 stars with precise T_{eff} , $[\text{Fe}/\text{H}]$, $[\alpha/\text{Fe}]$ and luminosity, which is defined as the total sample (hereafter TSample). By cross-matching the Tsample with the catalog of Santos et al. (2019, 2021) and removing the classical pulsator and close-in binary candidates (CP/CB), we obtain 7400 stars, including the rotation period (P_{rot}), variability amplitude (S_{ph}) and their corresponding errors named Sample I.

The R_{HK}^+ of dwarfs, derived based on the S-index, is an adequate proxy for the intensity of chromospheric

¹ https://gea.esac.esa.int/archive/documentation/GDR3/Data_analysis/chap_cu8par/sec_cu8par_apsis/ssec_cu8par_apsis_flame.html

² Reduced χ^2 of the spectral fit.

³ Flag indicating the selection of the spectrum with the highest S/N during repeated visits.

⁴ <https://www.aavso.org/vsx/>

Table 1. The summary of samples used in our work. The \checkmark indicates that all the sample stars have corresponding parameters.

Parameter	TSample	Sample I	Sample II
T_{eff} , [Fe/H], [α /Fe]	\checkmark	\checkmark	\checkmark
Luminosity	\checkmark	\checkmark	\checkmark
P_{rot}		\checkmark	
S_{ph}		\checkmark	
S index			\checkmark
R_{HK}^+			\checkmark
Volume	698885 stars	7400 stars	61701 stars

magnetic activity. The single observation for the measurement of the S-index is probably overestimated or underestimated in a long magnetic activity cycle. Therefore, we only adopt the stars with two or more observations from the TSample and then calculate the weighted average S-index by the following formula:

$$S = \frac{\sum^n S_L * SNR}{\sum^n SNR}, \quad (3)$$

where S_L is the S-index and SNR is signal to noise ratio, adopted by Zhang et al. (2022). Following the method of Mittag et al. (2013) to obtain R_{HK}^+ of stars. The specific formula is:

$$R_{HK}^+ = \frac{\mathcal{F}_{HK} - \mathcal{F}_{HK,phot} - \mathcal{F}_{HK,basal}}{\sigma \mathcal{T}_{eff}^4}, \quad (4)$$

where σ is the Stefan-Boltzmann constant, $\mathcal{F}_{HK,phot}$ is the photometric flux in Ca II H&K lines, and $\mathcal{F}_{HK,basal}$ is basal chromospheric flux. \mathcal{F}_{HK} is the arbitrary surface flux, defined by Middelkoop (1982):

$$\mathcal{F}_{HK} = 10^{8.25-1.67(B-V)} S, \quad (5)$$

where the B-V values are derived by the interpolation of T_{eff} and [Fe/H] (Ramírez & Meléndez 2005).

We obtain R_{HK}^+ of 61,701 stars, regarded as Sample II. In addition, to compare the chromospheric activity level of the Sun with G dwarfs, we converted solar S-index (0.179 - 0.194) on LAMOST scale (Zhang et al. 2020a) to solar $R_{HK}^+ \sim (1.209 - 1.600) * 10^{-5}$ according to the above process. All the samples used in our work are listed in Table 1.

3. FUNDAMENTAL PARAMETER ESTIMATION

3.1. Stellar Model Grid

Stellar model grid is a method for determining the fundamental characteristics of stars by generating a series of theoretical tracks with different metallicity, masses, and ages, and comparing them to observations such as

T_{eff} , $\log g$, [Fe/H] to determine the best-fit model. The α -enhanced stellar evolution model for this work is established in Sun et al. (2023), computed using the Modules for Experiments in Stellar Astrophysics (MESA) code (Paxton et al. 2011, 2013, 2015, 2018, 2019). The inlist file (for MESA) utilized in the computation of our stellar models is available on Zenodo at doi: [10.5281/zenodo.7866625](https://doi.org/10.5281/zenodo.7866625).

The mass range of this stellar model grid is from 0.7 M_{\odot} to 1.5 M_{\odot} with a grid step of 0.02 M_{\odot} . The input [Fe/H] values vary from -2.00 to $+0.45$ dex with a grid step of 0.05 dex. Additionally, the α -enhanced value ranges from 0.0 to 0.3 dex with a step size of 0.1 dex. The helium enrichment law was calibrated with initial abundances of helium and heavy elements of the standard solar model provided by Paxton et al. (2011), resulting in a helium-to-metal enrichment ratio of $Y = 0.248 + 1.3324Z$. The mixing-length parameter α_{MLT} is set to 1.82. In order to account for the effect of microscopic diffusion and gravitational settling of elements in low-mass stars, we employed the formulation of Thoul et al. (1994), which can modify the surface abundances and main-sequence lifetimes (Chaboyer et al. 2001; Bressan et al. 2012). We utilized the solar mixture GS98 (Grevesse & Sauval 1998) and supplemented the opacity tables with OPAL high-temperature opacities⁵ and low-temperature opacities (Ferguson et al. 2005). Other details about the input physics of our stellar models are presented in Sun et al. (2023).

3.2. Bayesian framework

We utilize Bayesian statistics (Basu et al. 2010) to infer stellar fundamental parameters by combining the prior knowledge of the model-given parameters with observed data. This is expressed as the posterior probability of a model M_i given data \mathcal{D} and prior information \mathcal{I} . The result is the posterior probability distribution of the model stellar parameters, $P(M_i|D, I)$.

$$P(M_i|D, I) = \frac{p(M_i|I)p(D|M_i)}{p(D|I)} \quad (6)$$

where $P(M_i|I)$ is the normalized prior probability of a particular model, which is equal to the reciprocal of the number of models $1/N_m$. Then:

$$\begin{aligned} P(D|M_i, I) &= L(T_{\text{eff}}, [Fe/H], Luminosity) \\ &= L_{T_{\text{eff}}} L_{[Fe/H]} L_{Luminosity} \end{aligned} \quad (7)$$

where L is the maximum likelihood function, in the form of:

$$L = \frac{1}{\sqrt{2\pi}\sigma} \exp \frac{-(\phi_{\text{obs}} - \phi_{\text{model}})^2}{2\sigma^2}, \quad (8)$$

⁵ <http://opalopacity.llnl.gov/new.html>

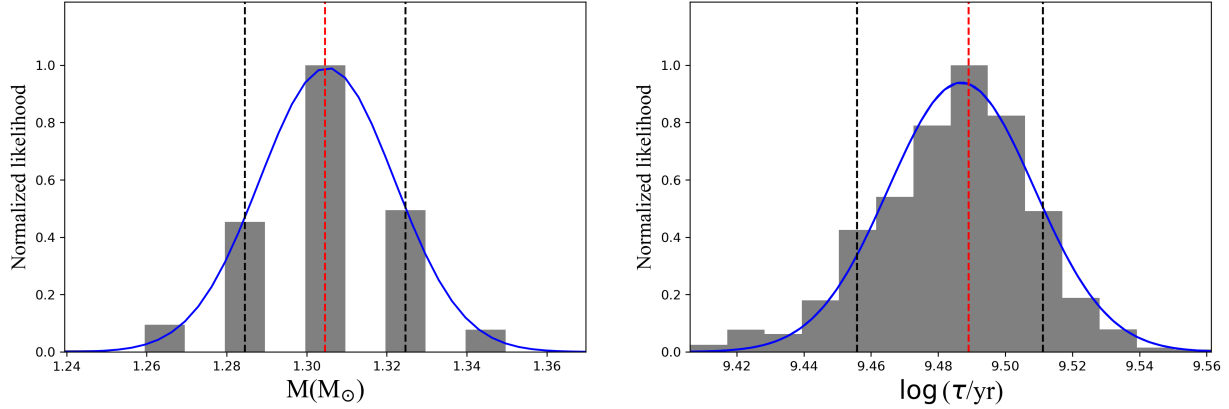


Figure 2. Likelihood distributions of mass and age in logarithmic scale for the example star, which is the common target of our sample and asteroseismic sample. The vertical red solid line represents the most probable value, while the black dashed lines indicate the probability values at the 0.16 and 0.84 quantities.

here σ is the error of the observation ϕ_{obs} .

The $p(D|I)$ in Eq.6 is a normalization factor for the specific model probability,

$$p(D|I) = \sum_{j=1}^{N_m} p(M_j|I)p(D|M_j, I) \quad (9)$$

The simplified version of the posterior probability is obtained by canceling the uniform priors:

$$p(M_i|D, I) = \frac{p(D|M_i, I)}{\sum_{j=1}^{N_m} p(D|M_j, I)}. \quad (10)$$

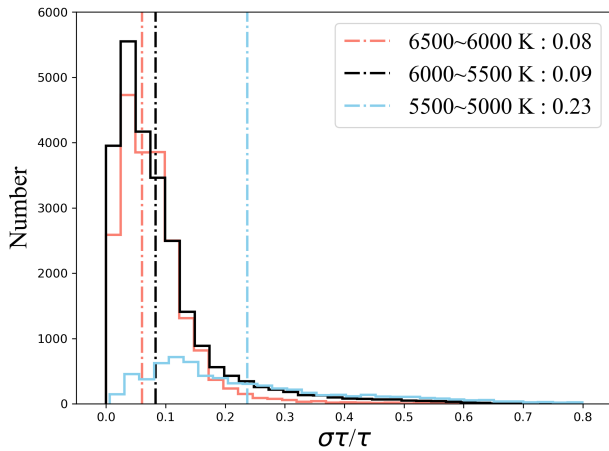


Figure 3. Age uncertainty of stars in different effective temperature intervals as labeled in legend.

The result provides the probability distribution for the selected models with the most likely fundamental parameters, and is plotted in Fig.2. Posterior probability distributions are constructed for each parameter to obtain estimation at the median, along with uncertainty expressed as standard deviation.

To evaluate the reliability of masses and ages in this study, we divide the sample into three temperature ranges of 500 K intervals. The results show that the mean of age precision for the 6500-6000 K, 6000-5500 K, and 5500-5000 K are 8%, 9%, and 23%, respectively, as shown in Fig.3. A total of 52,321 stars with reliable age uncertainty ($\sigma_\tau/\tau \leq 0.8$) and $\tau \leq 13.8$ Gyr are preserved, and the mean age uncertainty is 11%.

In addition, we cross-match our sample with the asteroseismic sample (Silva Aguirre et al. 2017; Serenelli et al. 2017), and obtain 137 common stars. We compare the masses and ages of these stars derived by seven pipelines with our results, as shown in Fig.4. The median absolute deviation (MAD) is listed in Table 2. Our results indicate a good agreement with the asteroseismic parameters.

Table 2. The Median Absolute Deviations (MAD) obtained from comparing our mass and age with those derived from six different pipelines.

Pipeline	MAD of age	MAD of mass
ASTFIT	2.52%	1.38%
BASTA	6.06%	2.36%
C2kSMO	5.10%	4.16%
GOE	25.68%	3.37%
V&A	4.19%	0.55%
YMCM	3.35%	1.77%
Serenelli17	3.13%	3.02%

NOTE—The details of the first six pipelines are described in Silva Aguirre et al. (2017) and the last pipeline in Serenelli et al. (2017).

4. RESULTS

We present a catalog of 52,321 stars with P_{rot} , S_{ph} , R_{HK}^+ , $[Fe/H]$, mass and age, listed in Table 4. To limit

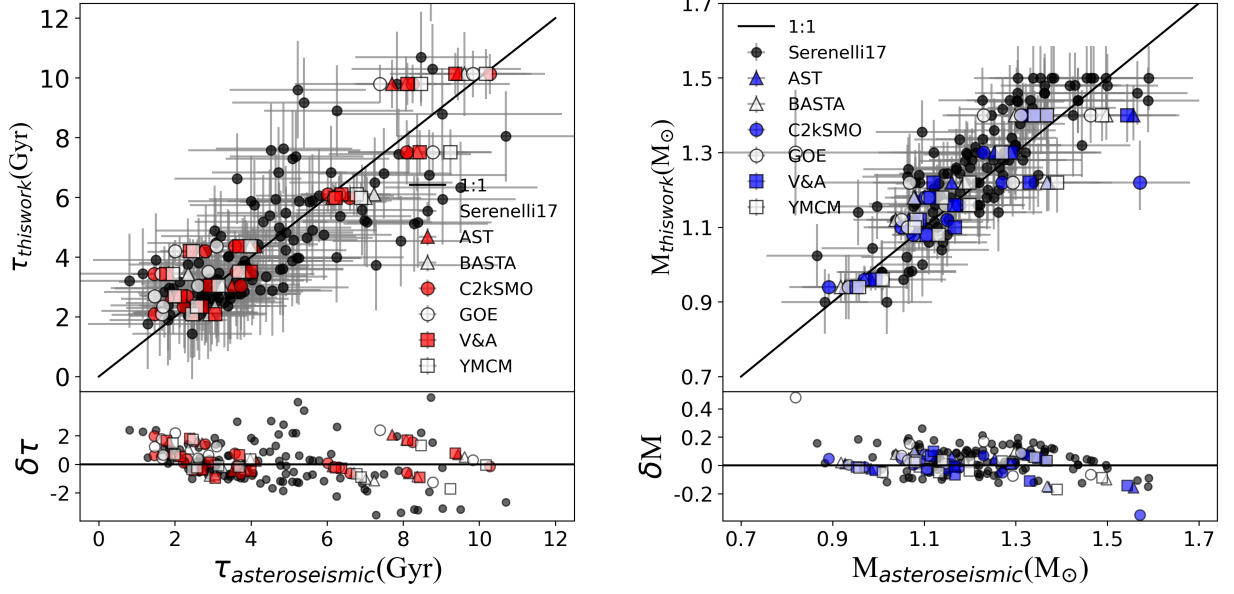


Figure 4. Comparison of fundamental parameters between this work and asteroseismic sample. The x-axis displays the mass and age values calculated using asteroseismic parameters. The solid lines represent the equal values of the parameters. Different symbols are used for different pipelines: solid triangle for AST, hollow triangle for BASTA, red spot for C2kSMO, circle for GOE, solid square for V&A, hollow square for YMCM, and black spot for Serenelli17. The short gray line is the error bar. The residuals are plotted on the Y-axis in the respective lower panels.

Table 3. Coefficient, intercept of linear fitting in Eq.11. Application range, Pearson correlation coefficient, the null hypothesis for each bin, the number of stars included in the fit, typical uncertainty of x- and y-axis in each panel.

y	Mass interval (M_{\odot})	[Fe/H] interval	α	β	Age range (Gyr)	r - value	p - value	N_{fit}	Age error (Gyr)	y error
P_{rot}	1.4 ~ 1.1	-1.0 ~ -0.1	1.750 ± 0.060	-15.850 ± 0.567	1-5	0.597	0.0	848	0.241	0.670
		-0.1 ~ 0.1	1.442 ± 0.029	-12.782 ± 0.274	1-6	0.816	0.0	1008	0.231	0.800
		0.1 ~ 0.5	1.132 ± 0.026	-9.707 ± 0.246	1-7	0.868	0.0	583	0.245	1.610
	1.1 ~ 0.9	-1.0 ~ -0.1	1.159 ± 0.042	-10.133 ± 0.412	2-11	0.590	0.0	733	0.631	1.480
		-0.1 ~ 0.1	0.731 ± 0.024	-5.857 ± 0.232	2-11	0.667	0.0	1151	0.835	1.800
		0.1 ~ 0.5	0.546 ± 0.024	-3.965 ± 0.23	2-11	0.645	0.0	591	0.850	2.210
	0.9 ~ 0.7	-1.0 ~ -0.1	0.106 ± 0.047	0.324 ± 0.463	2-13	0.024	0.207	397	1.403	2.290
		-0.1 ~ 0.1	0.285 ± 0.086	-1.494 ± 0.844	2-13	0.204	0.001	394	1.693	1.835
		0.1 ~ 0.5	0.334 ± 0.08	-1.839 ± 0.792	2-12	0.364	0.001	105	1.724	2.600
	1.4 ~ 1.1	-1.0 ~ -0.1	-0.548 ± 0.011	0.404 ± 0.106	1-6	-0.438	0.0	9954	0.186	0.012
		-0.1 ~ 0.1	-0.208 ± 0.010	-2.950 ± 0.099	1-7	-0.328	0.0	4960	0.197	0.012
		0.1 ~ 0.5	-0.149 ± 0.020	-3.532 ± 0.193	1-7	-0.207	0.0	1508	0.204	0.012
R_{HK}^+	1.1 ~ 0.9	-1.0 ~ -0.1	-0.119 ± 0.007	-3.679 ± 0.070	2-13	-0.147	0.0	11632	0.416	0.012
		-0.1 ~ 0.1	-0.449 ± 0.009	-0.495 ± 0.084	2-13	-0.397	0.0	6220	0.536	0.012
		0.1 ~ 0.5	-0.400 ± 0.018	-0.997 ± 0.182	2-13	-0.413	0.0	2257	0.544	0.013
	0.9 ~ 0.7	-1.0 ~ -0.1	-0.061 ± 0.017	-4.244 ± 0.166	3-13	0.015	0.365	6576	0.936	0.013
		-0.1 ~ 0.1	-0.671 ± 0.018	1.753 ± 0.182	2-13	-0.616	0.0	2026	1.216	0.013
		0.1 ~ 0.5	-0.651 ± 0.042	1.506 ± 0.416	2-13	-0.451	0.0	439	1.263	0.015

the relations among rotation, activity, metallicity, mass and age, we divide the sample into 9 bins according to their [Fe/H] and mass. Metallicity bins are classified as:

- sub-solar metallicity: $-1.0 \leq [Fe/H] < -0.1$,
- near-solar metallicity: $-0.1 \leq [Fe/H] < 0.1$,
- super-solar metallicity: $0.1 \leq [Fe/H] < 0.5$.

Stars at fixed metallicity bin are classified as:

- F dwarf: $1.4 - 1.1 M_{\odot}$,
- G dwarf: $1.1 - 0.9 M_{\odot}$,
- K dwarf: $0.9 - 0.7 M_{\odot}$.

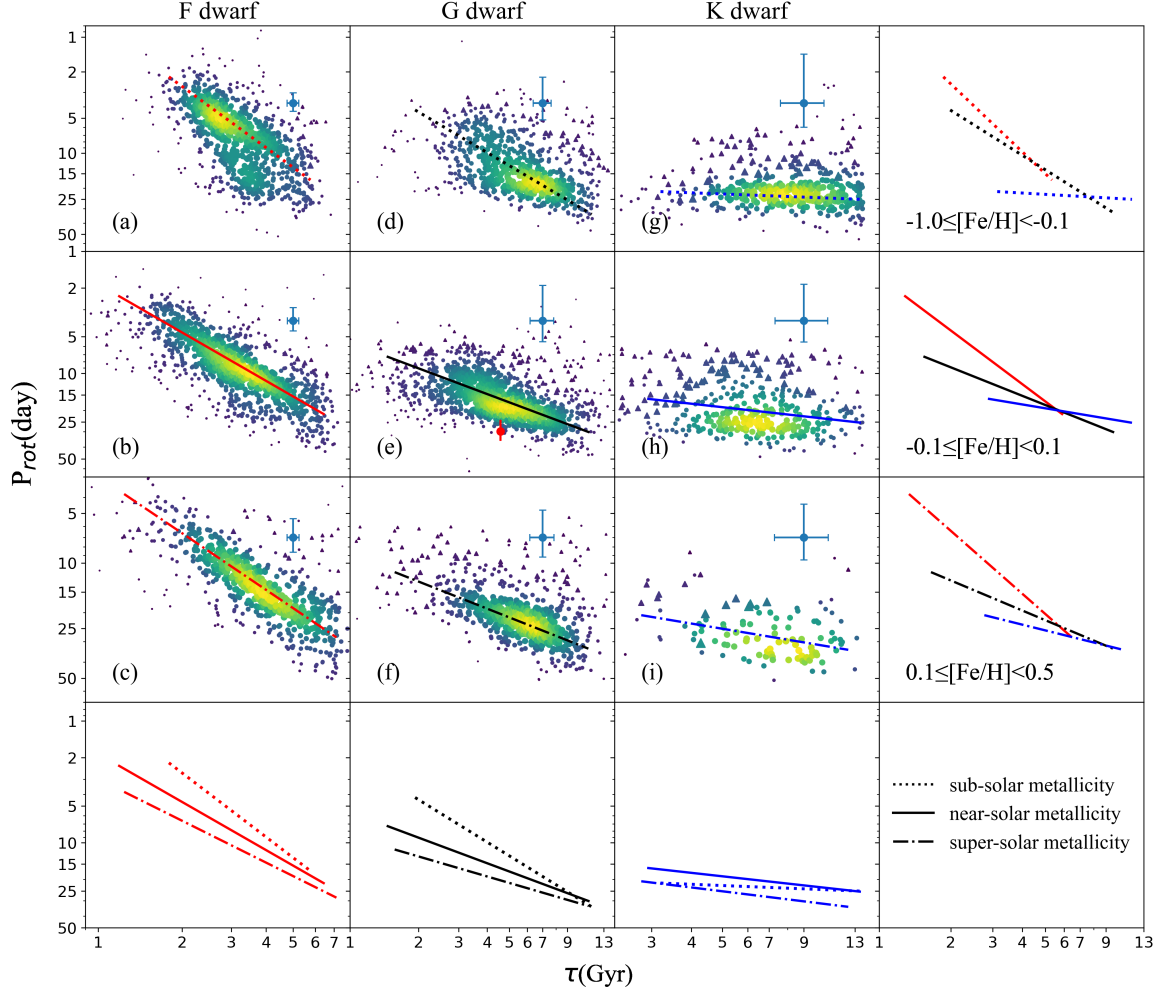


Figure 5. Distribution of rotation period with age for different spectral types, as indicated by the title. The segment linear fitting is represented by lines, with line colors corresponding to spectral type and line styles denoting distinct metallicity, as noted in the text. Scatter sizes as well as color reflect the data distribution density. The solar P_{rot} (24.47 ~ 35 day) and age (~ 4.57 Gyr) are marked by a red error bar in the central subplot. Blue error bar is the typical uncertainty of each bin. Triangles represent the $\log S_{ph} > 3.3$ in diffuse points (the data distribution density less than 16%).

Fig.5 and Fig.6 show the relations of $P_{rot}(\tau, M, [\text{Fe}/\text{H}])$ and $R_{HK}^+(\tau, M, [\text{Fe}/\text{H}])$, respectively. For each bin, we use the Pearson correlation coefficient (r-value) and the null hypothesis (p-value) to examine the potential connections between two parameters as displayed in Table 3. Note that the p-value for all bins is less than 0.05, which means the significant linear relation of $\log P_{rot} - \tau$ and $\log R_{HK}^+ - \tau$, except for K dwarfs with sub-solar metallicity greater than 0.05. Therefore we can employ a linear fitting model in the forms of the following:

$$\log y = \alpha \log \tau + \beta, \quad (11)$$

where y corresponds to the P_{rot} or R_{HK}^+ . τ is age in years. α is the slope, representing the spin-down rate in Fig.5 or the decay rate of $\log R_{HK}^+$ in Fig.6. β is the

intercept, representing the constant for each bin. The best fits are listed in Table 3. To ensure the robustness of our fitting results, we weigh our fitting with the data distribution density.

The optimal fit is achieved by minimizing the weighted sum of residuals, $r(\theta)$.

$$r(\theta) = \sum_{i=1}^N w_i (y_i - f(x_i, \theta))^2, \quad (12)$$

Where N is the number of data points. x_i and y_i are the data point. θ represents the free parameter. w_i is the weight, which is determined by the data distribution density. In this work, we sorted stars by age and computed the data distribution density using the Gaussian kernel density estimation (Scott 2015) for individual

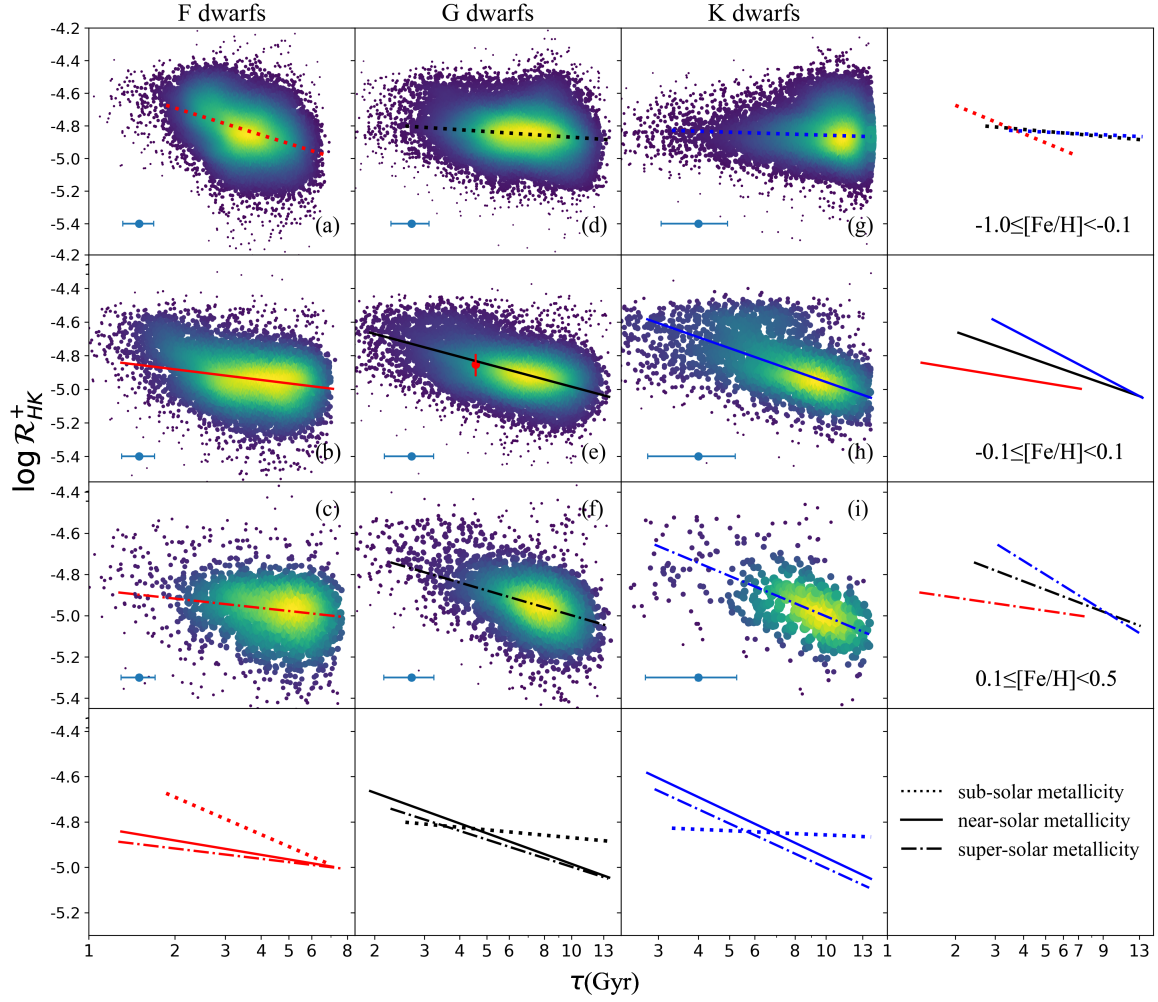


Figure 6. Consistent with Fig.5, except that the y-axis is the chromospheric activity indices, and solar $R_{HK}^+ \sim (1.209 - 1.600) * 10^{-5}$.

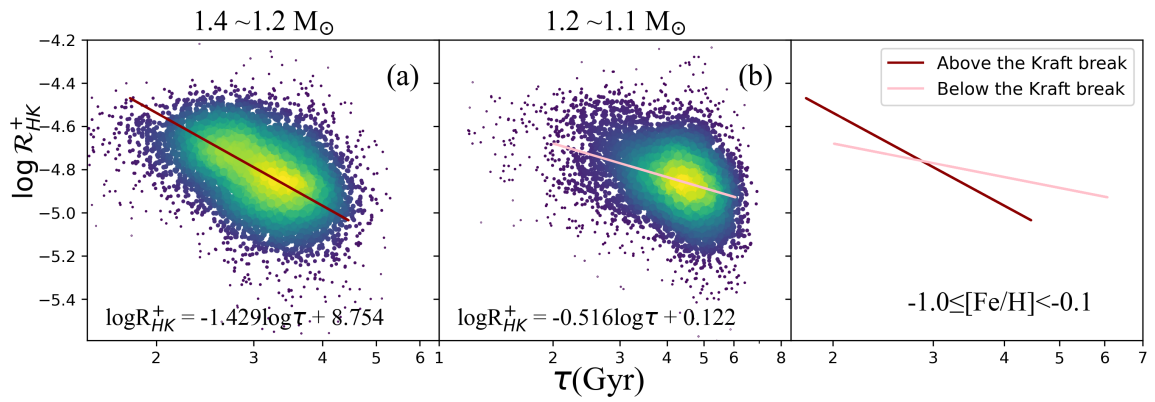


Figure 7. The sub-bins of Fig.6(a), the title indicates the mass range of stars and the fitting results as shown as text and solid line.

points within 3σ :

$$\hat{f}(x) = \frac{1}{Nh} \sum_{i=1}^N \frac{1}{\sqrt{2\pi}} \exp \frac{-(x-x_i)^2}{2h^2}, \quad (13)$$

where h is the bandwidth that controls the width of the Gaussian kernel.

$$4.1. P_{rot}(\tau, M, [Fe/H])$$

Table 4. Columns overview of the Sample.

Parameter	Format	Units	Description
Source	long	–	Gaia DR3 ID
RA	float	deg	Right ascension (J2000)
DEC	float	deg	Declination (J2000)
SNR_G	float	–	Spectral S/N per pixel in SDSS g band
Teff	float	K	Effective temperature
Teff_err	float	K	Uncertainty in Teff
logg	float	dex	Log of surface gravity
logg_err	float	dex	Uncertainty in logg
FeH	float	dex	Iron abundance
FeH_err	float	dex	Uncertainty in FeH
Alpha_Fe	float	dex	Alpha element to iron abundance ratio
Alpha_Fe_err	float	dex	Uncertainty in Alpha_Fe
Gmag	float	mag	Absolute magnitude in Gaia G band
Gmag_err	float	mag	Standard error of Gmag
Lum_Flame	float	L_{\odot}	Stellar luminosity with FLAME pipeline
Lum_Flame_err	float	L_{\odot}	Standard error of Lum_Flame
KIC	int	–	Kepler Input Catalog ID
Prot	float	day	Rotation Period
E_Prot	float	day	Uncertainty in Prot
Sph	float	ppm	Amplitude brightness variations
E_Sph	float	ppm	Uncertainty in Sph
S_index	float	–	Weight average value of S_L index
S_err	float	–	Uncertainty in S-index
SNR	float	–	S-index S/N
logRHKplus	float	–	Chromospheric activity index
logRHKplus_err	float	–	Uncertainty in RHKplus
Mass	float	M_{\odot}	Mass with grid-based modelling
Mass_err	float	M_{\odot}	Uncertainty in Mass
Age	float	Gyr	Age with gridbased modelling
Age_err	float	Gyr	Uncertainty in Age

NOTE—The comparison of Mass and T_{eff} in our sample with those from Santos et al. (2019, 2021) indicate that the MAD is ~ 101 K, with a dispersion ~ 172 K for T_{eff} ; the MAD is $\sim 0.015 M_{\odot}$, with a dispersion value $\sim 0.065 M_{\odot}$ for Mass.

According to the correlation test and the slope of linear fitting, we find a pronounced relation among P_{rot} , metallicity, mass and age, as shown in Fig. 5. For FG dwarfs in Fig. 5(a-c) and Fig. 5(d-f), the results clearly indicate that: i) P_{rot} increase with increasing age within a range of 1-7 Gyr for F dwarfs, and 2-11 Gyr for G dwarfs, respectively; ii) the spin-down rate of F dwarfs is larger than that of G dwarfs; iii) stars with sub-solar metallicity tend to rotate faster and have the larger spin-down rate than the ones with super-solar metallicity at given mass bin. This suggests that the spin-down torque is affected by metallicity, i.e. opacity increases with metallicity, resulting in a deeper convective envelope and greater loss rate of angular momentum for metal-poor stars at the given masses (Amard et al. 2020). In Fig. 5(e), we notice that the solar P_{rot} (24.47 \sim 35 days) is larger than the median value of other stars, which is probably associated with the detection threshold of Kepler. It will be discussed in Section 4.2.

For K dwarfs in Fig. 5(g-i), we find that: i) the correlation between age and P_{rot} is not significant; ii) there are a fraction of fast rotators ($P_{\text{rot}} < 20$ days) with high

variability amplitudes ($\log S_{\text{ph}} > 3.3$), especially for K dwarfs, which may be affected by high activity level and large intrinsic stellar noise (Christiansen et al. 2012; Masuda 2022). iii) a notable dense region appears in $P_{\text{rot}} \sim 25$ days, indicative of low activity levels. This flat region in the longer period of K dwarfs may be a crucial prediction for the weakened magnetic braking (van Saders et al. 2016; David et al. 2022).

4.2. $R_{HK}^+(\tau, M, [Fe/H])$

The chromospheric activity levels decrease with increasing age, but the correlation of $\log R_{HK}^+ - \tau$ differs due to mass and metallicity, as displayed in Fig. 6. F dwarfs with sub-solar metallicity present a prominent negative correlation in the range of 2-6 Gyr as shown in Fig. 6(a). Ones with $[Fe/H] > -0.1$, the correlation of $\log R_{HK}^+ - \tau$ is not significant, as illustrated in Fig. 6(b-c). The metal-poor stars have shallower Ca II H&K profiles that correspond to higher levels of R_{HK}^+ (Rocha-Pinto & Maciel 1998; Lorenzo-Oliveira et al. 2016).

For G dwarfs in Fig. 6(d-f), there is a clear correlation between $\log R_{HK}^+$ and age within the range of 2-13 Gyr.

As shown in Fig.6(e), the activity level of the Sun is comparable to that of G dwarfs with age near 4.5 Gyr, aligned with the previous findings (Wright et al. 2004; Sreejith et al. 2020; Gomes da Silva et al. 2021). This means the Sun is a normal star at the stage, which likely contradicts the result of Fig.5(e). This suggests that it is difficult to detect the P_{rot} of stars with solar activity level in Kepler data (Zhang et al. 2020b). In addition, we select stars with masses ranging from 0.98 to 1.02 M_{\odot} and metallicity in the range -0.05 to 0.05 dex, then give the slope of activity-age relation. We find our slope ~ -0.53 is similar to that ~ -0.52 from Lorenzo-Oliveira et al. (2018).

In Fig.6(g-i), K dwarfs exhibit the most noticeable decay rate of $\log R_{HK}^+$ for the stars with $[\text{Fe}/\text{H}] > -0.1$ than that of FG dwarfs in a range of 3-13 Gyr. The trend has been identified in open clusters as reported by Zhang et al. (2019), where later-type dwarfs exhibit a more pronounced trend of $\log R_{HK}^+ - \tau$. This means that $\log R_{HK}^+$ is a powerful age probe for K dwarfs when the $P_{rot} - \tau$ fails. In addition, our results prove the feasibility of the chromospheric activity index as an age indicator for old field stars (Metcalfe & Egeland 2019).

Sub-solar metallicity F dwarfs exhibit an exceptionally larger decay rate of chromospheric activity than other stars with similar spectral types or metallicity. Since their surface convection zone is very thin, we need to consider the impact from the stars above the Kraft break (Kraft 1967), therefore we further subdivide the stars in this interval into two mass bins (1.4-1.2, 1.2-1.1 M_{\odot}), which corresponding to above the Kraft break (Fig.7(a)) and below the Kraft break (Fig.7(b)). Fig.7 reveals that the decay rate of $\log R_{HK}^+$ is stronger for more massive or hotter stars, but the slope becomes smaller for stars below the Kraft break. The difference between the slopes confirms that the stars above the Kraft break ($M > 1.2 M_{\odot}$) are probably associated with the strong negative correlation in Fig.6(a).

5. CONCLUSION

To calibrate the relations of $P_{rot}(\tau, M, [\text{Fe}/\text{H}])$ and $R_{HK}^+(\tau, M, [\text{Fe}/\text{H}])$, we constructed a catalog of 52,321 FGK dwarfs, with T_{eff} , $[\text{Fe}/\text{H}]$, M_G , L/L_{\odot} , $[\alpha/\text{Fe}]$, P_{rot} , S_{ph} , R_{HK}^+ , mass and age, etc. Our results demonstrate:

- For F dwarfs, there is a clear relation among P_{rot} , age, and $[\text{Fe}/\text{H}]$ in the range of 1-7 Gyr. However, the decrease of $\log R_{HK}^+$ over time is not significant except for those with $[\text{Fe}/\text{H}] < -0.1$.
- For G dwarfs, both the correlation of $P_{rot} - \tau$ and $\log R_{HK}^+ - \tau$ are significant in the ranges 2-11 and

2-13 Gyr, respectively. This suggests that P_{rot} and $\log R_{HK}^+$ are reliable age probes.

- For K dwarfs, they behave the weakest correlation of $P_{rot} - \tau$. However, they exhibit the most prominent correlation of $\log R_{HK}^+ - \tau$ than that of FG dwarfs within the age range of 3-13 Gyr.
- For the Sun, we confirm it has a comparable activity level with other G dwarfs at the given age.

We find that P_{rot} is a reliable age indicator for FG dwarfs, while $\log R_{HK}^+$ is a powerful age probe for GK dwarfs, based on the relations of $P_{rot}([\text{Fe}/\text{H}], M, \tau)$ and $R_{HK}^+([\text{Fe}/\text{H}], M, \tau)$. The calibrated relations expand the application of gyrochronology to 11 Gyr and magnetochronology to 13 Gyr. The results are promising in quick age estimation for the larger dwarf sample in forthcoming photometric and spectroscopic surveys.

This work is supported by the Joint Research Fund in Astronomy (U2031203) under cooperative agreement between the National Natural Science Foundation of China (NSFC) and Chinese Academy of Sciences (CAS), and NSFC grants (12090040, 12090042). J.-H.Z. acknowledges support from NSFC grant No.12103063. This work is partially supported by the Scholar Program of Beijing Academy of Science and Technology (DZ:BS202002) and the CSST project. M.X. acknowledges China National Key R&D Program No.2022YFF0504200 and NSFC grant No.2022000083 for financial support for the computation of LAMOST spectroscopic stellar parameters with DD-Payne.

This work is based on data from the Guoshoujing Telescope (the Large Sky Area Multi-Object Fiber Spectroscopic Telescope LAMOST). Funding for the project has been provided by the National Development and Reform Commission. LAMOST is operated and managed by the National Astronomical Observatories, Chinese Academy of Sciences. This work has made use of data from the European Space Agency (ESA) mission Gaia (<https://www.cosmos.esa.int/gaia>), processed by the Gaia Data Processing and Analysis Consortium (DPAC, <https://www.cosmos.esa.int/web/gaia/dpac/consortium>). Funding for the DPAC has been provided by national institutions, in particular, the institutions participating in the Gaia Multilateral Agreement. This paper includes data collected by the Kepler mission. Funding for the Kepler mission was provided by the NASA Science Mission directorate. M.X. acknowledges China National Key R&D Program No. 2022YFF0504200 and NSFC grant No. 2022000083 for financial support for the computation of LAMOST spectroscopic stellar parameters with DD-Payne.

REFERENCES

- Amard, L., Roquette, J., & Matt, S. P. 2020, *MNRAS*, 499, 3481, doi: [10.1093/mnras/staa3038](https://doi.org/10.1093/mnras/staa3038)
- Angus, R., Aigrain, S., Foreman-Mackey, D., & McQuillan, A. 2015, *MNRAS*, 450, 1787, doi: [10.1093/mnras/stv423](https://doi.org/10.1093/mnras/stv423)
- Angus, R., Morton, T. D., Foreman-Mackey, D., et al. 2019, *AJ*, 158, 173, doi: [10.3847/1538-3881/ab3c53](https://doi.org/10.3847/1538-3881/ab3c53)
- Barnes, S. A. 2003, *ApJ*, 586, 464, doi: [10.1086/367639](https://doi.org/10.1086/367639)
- . 2007, *ApJ*, 669, 1167, doi: [10.1086/519295](https://doi.org/10.1086/519295)
- . 2010, *ApJ*, 722, 222, doi: [10.1088/0004-637X/722/1/222](https://doi.org/10.1088/0004-637X/722/1/222)
- Basri, G., Walkowicz, L. M., Batalha, N., et al. 2011, *AJ*, 141, 20, doi: [10.1088/0004-6256/141/1/20](https://doi.org/10.1088/0004-6256/141/1/20)
- Basu, S., Chaplin, W. J., & Elsworth, Y. 2010, *ApJ*, 710, 1596, doi: [10.1088/0004-637X/710/2/1596](https://doi.org/10.1088/0004-637X/710/2/1596)
- Booth, R. S., Poppenhaeger, K., Watson, C. A., et al. 2020, *MNRAS*, 491, 455, doi: [10.1093/mnras/stz3039](https://doi.org/10.1093/mnras/stz3039)
- Bressan, A., Marigo, P., Girardi, L., et al. 2012, *MNRAS*, 427, 127, doi: [10.1111/j.1365-2966.2012.21948.x](https://doi.org/10.1111/j.1365-2966.2012.21948.x)
- Bressan, A., Marigo, P., Girardi, L., et al. 2012, *Monthly Notices of the Royal Astronomical Society*, 427, 127, doi: [10.1111/j.1365-2966.2012.21948.x](https://doi.org/10.1111/j.1365-2966.2012.21948.x)
- Chaboyer, B., Fenton, W. H., Nelan, J. E., Patnaude, D. J., & Simon, F. E. 2001, *ApJ*, 562, 521, doi: [10.1086/323872](https://doi.org/10.1086/323872)
- Choi, J., Dotter, A., Conroy, C., et al. 2016, *ApJ*, 823, 102, doi: [10.3847/0004-637X/823/2/102](https://doi.org/10.3847/0004-637X/823/2/102)
- Christiansen, J. L., Jenkins, J. M., Caldwell, D. A., et al. 2012, *PASP*, 124, 1279, doi: [10.1086/668847](https://doi.org/10.1086/668847)
- Curtis, J. L., Agüeros, M. A., Douglas, S. T., & Meibom, S. 2019, *ApJ*, 879, 49, doi: [10.3847/1538-4357/ab2393](https://doi.org/10.3847/1538-4357/ab2393)
- Curtis, J. L., Agüeros, M. A., Matt, S. P., et al. 2020, *ApJ*, 904, 140, doi: [10.3847/1538-4357/abbf58](https://doi.org/10.3847/1538-4357/abbf58)
- David, T. J., Angus, R., Curtis, J. L., et al. 2022, *ApJ*, 933, 114, doi: [10.3847/1538-4357/ac6dd3](https://doi.org/10.3847/1538-4357/ac6dd3)
- Dotter, A., Chaboyer, B., Jevremović, D., et al. 2008, *ApJS*, 178, 89, doi: [10.1086/589654](https://doi.org/10.1086/589654)
- Dunee, R., van Saders, J., Gaidos, E., et al. 2022, *ApJ*, 938, 118, doi: [10.3847/1538-4357/ac90be](https://doi.org/10.3847/1538-4357/ac90be)
- Ferguson, J. W., Alexander, D. R., Allard, F., et al. 2005, *ApJ*, 623, 585, doi: [10.1086/428642](https://doi.org/10.1086/428642)
- Gaia Collaboration, Vallenari, A., & Brown. 2022, arXiv e-prints, arXiv:2208.00211. <https://arxiv.org/abs/2208.00211>
- García, R. A., Ceillier, T., Salabert, D., et al. 2014, *A&A*, 572, A34, doi: [10.1051/0004-6361/201423888](https://doi.org/10.1051/0004-6361/201423888)
- Gomes da Silva, J., Santos, N. C., Adibekyan, V., et al. 2021, *A&A*, 646, A77, doi: [10.1051/0004-6361/202039765](https://doi.org/10.1051/0004-6361/202039765)
- Grevesse, N., & Sauval, A. J. 1998, *SSRv*, 85, 161, doi: [10.1023/A:1005161325181](https://doi.org/10.1023/A:1005161325181)
- Gustafsson, B., Edvardsson, B., Eriksson, K., et al. 2008, *A&A*, 486, 951, doi: [10.1051/0004-6361:200809724](https://doi.org/10.1051/0004-6361:200809724)
- Kawaler, S. D. 1988, *ApJ*, 333, 236, doi: [10.1086/166740](https://doi.org/10.1086/166740)
- Kraft, R. P. 1967, *ApJ*, 150, 551, doi: [10.1086/149359](https://doi.org/10.1086/149359)
- Long, L., Bi, S., Zhang, J., et al. 2023, arXiv e-prints, arXiv:2307.06596, doi: [10.48550/arXiv.2307.06596](https://doi.org/10.48550/arXiv.2307.06596)
- Lorenzo-Oliveira, D., Porto de Mello, G. F., & Schiavon, R. P. 2016, *A&A*, 594, L3, doi: [10.1051/0004-6361/201629233](https://doi.org/10.1051/0004-6361/201629233)
- Lorenzo-Oliveira, D., Freitas, F. C., Meléndez, J., et al. 2018, *A&A*, 619, A73, doi: [10.1051/0004-6361/201629294](https://doi.org/10.1051/0004-6361/201629294)
- Mamajek, E. E., & Hillenbrand, L. A. 2008, *ApJ*, 687, 1264, doi: [10.1086/591785](https://doi.org/10.1086/591785)
- Masuda, K. 2022, *ApJ*, 933, 195, doi: [10.3847/1538-4357/ac7527](https://doi.org/10.3847/1538-4357/ac7527)
- Mathur, S., García, R. A., Ballot, J., et al. 2014, *A&A*, 562, A124, doi: [10.1051/0004-6361/201322707](https://doi.org/10.1051/0004-6361/201322707)
- Matt, S., & Pudritz, R. E. 2005, *ApJL*, 632, L135, doi: [10.1086/498066](https://doi.org/10.1086/498066)
- Matt, S. P., Brun, A. S., Baraffe, I., Bouvier, J., & Chabrier, G. 2015, *ApJL*, 799, L23, doi: [10.1088/2041-8205/799/2/L23](https://doi.org/10.1088/2041-8205/799/2/L23)
- McQuillan, A., Aigrain, S., & Mazeh, T. 2013, *MNRAS*, 432, 1203, doi: [10.1093/mnras/stt536](https://doi.org/10.1093/mnras/stt536)
- McQuillan, A., Mazeh, T., & Aigrain, S. 2014, *ApJS*, 211, 24, doi: [10.1088/0067-0049/211/2/24](https://doi.org/10.1088/0067-0049/211/2/24)
- Meibom, S., Barnes, S. A., Latham, D. W., et al. 2011, *ApJL*, 733, L9, doi: [10.1088/2041-8205/733/1/L9](https://doi.org/10.1088/2041-8205/733/1/L9)
- Metcalfe, T. S., & Egeland, R. 2019, *ApJ*, 871, 39, doi: [10.3847/1538-4357/aaf575](https://doi.org/10.3847/1538-4357/aaf575)
- Metcalfe, T. S., Strassmeier, K. G., Ilyin, I. V., et al. 2023, *ApJL*, 948, L6, doi: [10.3847/2041-8213/acce38](https://doi.org/10.3847/2041-8213/acce38)
- Middelkoop, F. 1982, *A&A*, 107, 31
- Mittag, M., Schmitt, J., & Schröder, K.-P. 2013, *Astronomy & Astrophysics*, 549, A117
- Moser, S., Valle, G., Dell'Omodarme, M., Degl'Innocenti, S., & Prada Moroni, P. G. 2023, *A&A*, 671, A78, doi: [10.1051/0004-6361/202243897](https://doi.org/10.1051/0004-6361/202243897)
- Noyes, R. W., Hartmann, L. W., Baliunas, S. L., Duncan, D. K., & Vaughan, A. H. 1984, *ApJ*, 279, 763, doi: [10.1086/161945](https://doi.org/10.1086/161945)
- Paxton, B., Bildsten, L., Dotter, A., et al. 2011, *ApJS*, 192, 3, doi: [10.1088/0067-0049/192/1/3](https://doi.org/10.1088/0067-0049/192/1/3)
- Paxton, B., Cantiello, M., Arras, P., et al. 2013, *ApJS*, 208, 4, doi: [10.1088/0067-0049/208/1/4](https://doi.org/10.1088/0067-0049/208/1/4)
- Paxton, B., Marchant, P., Schwab, J., et al. 2015, *ApJS*, 220, 15, doi: [10.1088/0067-0049/220/1/15](https://doi.org/10.1088/0067-0049/220/1/15)
- Paxton, B., Schwab, J., Bauer, E. B., et al. 2018, *ApJS*, 234, 34, doi: [10.3847/1538-4365/aaa5a8](https://doi.org/10.3847/1538-4365/aaa5a8)
- Paxton, B., Smolec, R., Schwab, J., et al. 2019, *ApJS*, 243, 10, doi: [10.3847/1538-4365/ab2241](https://doi.org/10.3847/1538-4365/ab2241)

- Perini, S., Muttoni, G., Monesi, E., Melis, R. T., & Mussi, M. 2021, *Quaternary Science Reviews*, 274, 107259, doi: [10.1016/j.quascirev.2021.107259](https://doi.org/10.1016/j.quascirev.2021.107259)
- Petigura, E. A., Rogers, J. G., Isaacson, H., et al. 2022, *AJ*, 163, 179, doi: [10.3847/1538-3881/ac51e3](https://doi.org/10.3847/1538-3881/ac51e3)
- Ramírez, I., & Meléndez, J. 2005, *ApJ*, 626, 465, doi: [10.1086/430102](https://doi.org/10.1086/430102)
- Reinhold, T., & Gizon, L. 2015, *A&A*, 583, A65, doi: [10.1051/0004-6361/201526216](https://doi.org/10.1051/0004-6361/201526216)
- Réville, V., Folsom, C. P., Strugarek, A., & Brun, A. S. 2016, *ApJ*, 832, 145, doi: [10.3847/0004-637X/832/2/145](https://doi.org/10.3847/0004-637X/832/2/145)
- Rocha-Pinto, H. J., & Maciel, W. J. 1998, *MNRAS*, 298, 332, doi: [10.1046/j.1365-8711.1998.01597.x](https://doi.org/10.1046/j.1365-8711.1998.01597.x)
- Rybizki, J., Green, G. M., Rix, H.-W., et al. 2022, *Monthly Notices of the Royal Astronomical Society*, 510, 2597
- Santos, A. R. G., Breton, S. N., Mathur, S., & García, R. A. 2021, *ApJS*, 255, 17, doi: [10.3847/1538-4365/ac033f](https://doi.org/10.3847/1538-4365/ac033f)
- Santos, A. R. G., García, R. A., Mathur, S., et al. 2019, *ApJS*, 244, 21, doi: [10.3847/1538-4365/ab3b56](https://doi.org/10.3847/1538-4365/ab3b56)
- Schaerer, D., Meynet, G., Maeder, A., & Schaller, G. 1993, *A&AS*, 98, 523
- Scott, D. W. 2015, *Multivariate density estimation: theory, practice, and visualization* (John Wiley & Sons)
- Serenelli, A., Johnson, J., Huber, D., et al. 2017, *ApJS*, 233, 23, doi: [10.3847/1538-4365/aa97df](https://doi.org/10.3847/1538-4365/aa97df)
- Silva Aguirre, V., Lund, M. N., Antia, H. M., et al. 2017, *ApJ*, 835, 173, doi: [10.3847/1538-4357/835/2/173](https://doi.org/10.3847/1538-4357/835/2/173)
- Skumanich, A. 1972, *ApJ*, 171, 565, doi: [10.1086/151310](https://doi.org/10.1086/151310)
- Soderblom, D. R. 2010, *ARA&A*, 48, 581, doi: [10.1146/annurev-astro-081309-130806](https://doi.org/10.1146/annurev-astro-081309-130806)
- Sreejith, A. G., Fossati, L., Youngblood, A., France, K., & Ambily, S. 2020, *A&A*, 644, A67, doi: [10.1051/0004-6361/202039167](https://doi.org/10.1051/0004-6361/202039167)
- Sun, T., Ge, Z., Chen, X., et al. 2023, arXiv e-prints, arXiv:2307.04086, doi: [10.48550/arXiv.2307.04086](https://doi.org/10.48550/arXiv.2307.04086)
- Thoul, A. A., Bahcall, J. N., & Loeb, A. 1994, *ApJ*, 421, 828, doi: [10.1086/173695](https://doi.org/10.1086/173695)
- van Saders, J. L., Ceillier, T., Metcalfe, T. S., et al. 2016, *Nature*, 529, 181, doi: [10.1038/nature16168](https://doi.org/10.1038/nature16168)
- Vidotto, A. A., Gregory, S. G., Jardine, M., et al. 2014, *MNRAS*, 441, 2361, doi: [10.1093/mnras/stu728](https://doi.org/10.1093/mnras/stu728)
- Wright, J. T., Marcy, G. W., Butler, R. P., & Vogt, S. S. 2004, *ApJS*, 152, 261, doi: [10.1086/386283](https://doi.org/10.1086/386283)
- Xiang, M., Ting, Y.-S., Rix, H.-W., et al. 2019, *ApJS*, 245, 34, doi: [10.3847/1538-4365/ab5364](https://doi.org/10.3847/1538-4365/ab5364)
- Yi, S., Demarque, P., Kim, Y.-C., et al. 2001, *ApJS*, 136, 417, doi: [10.1086/321795](https://doi.org/10.1086/321795)
- Zhang, J., Zhao, J., Oswalt, T. D., et al. 2019, *ApJ*, 887, 84, doi: [10.3847/1538-4357/ab4efe](https://doi.org/10.3847/1538-4357/ab4efe)
- Zhang, J., Bi, S., Li, Y., et al. 2020a, *ApJS*, 247, 9, doi: [10.3847/1538-4365/ab6165](https://doi.org/10.3847/1538-4365/ab6165)
- Zhang, J., Shapiro, A. I., Bi, S., et al. 2020b, *ApJL*, 894, L11, doi: [10.3847/2041-8213/ab8795](https://doi.org/10.3847/2041-8213/ab8795)
- Zhang, W., Zhang, J., He, H., et al. 2022, *ApJS*, 263, 12, doi: [10.3847/1538-4365/ac9406](https://doi.org/10.3847/1538-4365/ac9406)
- Zhao, G., Zhao, Y.-H., Chu, Y.-Q., Jing, Y.-P., & Deng, L.-C. 2012, *Research in Astronomy and Astrophysics*, 12, 723, doi: [10.1088/1674-4527/12/7/002](https://doi.org/10.1088/1674-4527/12/7/002)